

# Black-Box Forgery Attacks on Semantic Watermarks for Diffusion Models

Andreas Müller, Denis Lukovnikov, Jonas Thietke, Asja Fischer\*, Erwin Quiring\*  
Ruhr University Bochum

## Abstract

Integrating watermarking into the generation process of latent diffusion models (LDMs) simplifies detection and attribution of generated content. Semantic watermarks, such as Tree-Rings and Gaussian Shading, represent a novel class of watermarking techniques that are easy to implement and highly robust against various perturbations. However, our work demonstrates a fundamental security vulnerability of semantic watermarks. We show that attackers can leverage unrelated models, even with different latent spaces and architectures (UNet vs DiT), to perform powerful and realistic forgery attacks. Specifically, we design two watermark forgery attacks. The first imprints a targeted watermark into real images by manipulating the latent representation of an arbitrary image in an unrelated LDM to get closer to the latent representation of a watermarked image. We also show that this technique can be used for watermark removal. The second attack generates new images with the target watermark by inverting a watermarked image and re-generating it with an arbitrary prompt. Both attacks just need a single reference image with the target watermark. Overall, our findings question the applicability of semantic watermarks by revealing that attackers can easily forge or remove these watermarks under realistic conditions.

## 1. Introduction

Recent advancements in generative AI, especially latent diffusion models (LDMs), have made it extremely challenging to distinguish between authentic and AI-generated images. Despite a multitude of beneficial applications, this also introduces a considerable range of threats. For example, so-called deepfakes—compellingly realistic but AI-generated media—are now routinely used to defraud people, distribute misinformation, and to manipulate public opinion [11, 15].

Thus, there is an urgent *need to detect and to attribute AI-generated images*, that is, to identify that an image is AI-generated and to determine who used the AI system to gener-

\*Equal supervision

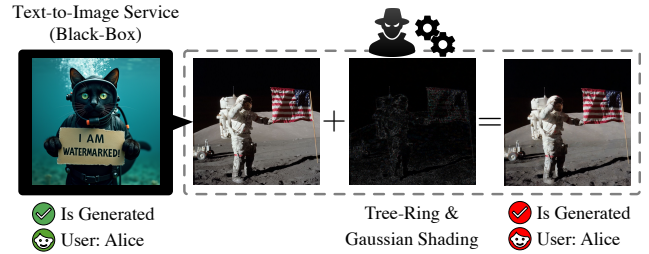


Figure 1. Semantic watermark forgery. The attacker can transfer the watermark from a watermarked reference image requested by Alice (here: the diving cat) into any cover image (here: the moon landing). The obtained image will be detected as watermarked and attributed to Alice by the service provider, eroding the trust in watermark-based detection and attribution of AI-generated content.

ate it. Watermarking is currently one of the main approaches for achieving these goals, and leading AI companies such as Google and Meta, as well as AI platforms such as Hugging Face and Google Gemini, are either already using it or have made commitments to do so [2, 8, 16, 19].

Recently, a novel family of watermarking methods for LDMs has been proposed that relies on the inversion of the denoising process in the diffusion model [7, 17, 38, 42]. These *semantic watermarks* work by modifying the initial latent noise to contain a specific watermark pattern which can be recovered through inversion of the denoising process. Semantic watermarks offer several advantages. First, they assert greater robustness against various image transformations and attacks compared to previous watermarking methods. Moreover, the DM remains unchanged, which makes the watermarking approach easy to deploy. However, it is critical that these watermarks are also secure against forgery attacks. Fig. 1 illustrates this threat where an attacker transfers the watermark of a service provider to any image. This can lead to an erosion of trust in the watermarking system, as real images are flagged as watermarked and thus AI-generated or regular users are blamed for distributing harmful content.

In this work, we uncover a fundamental security weakness of semantic watermarks. We demonstrate that attackers can use unrelated models, even with a different latent space

and architecture, to perform highly effective forgery attacks. These attacks just need a single reference image with the target watermark. Specifically, we propose two forgery strategies: (1) Our *imprinting attack* operates in the latent space of the attacker model where it reduces the distance between the latent representation of a watermarked and a clean cover image. The reduced distance also transfers to the latent space of the target model, effectively carrying over the watermark. We also adjust this method for watermark removal. (2) Our *reprompting* attack allows generating arbitrary images with the target watermark by inverting a watermarked image and re-generating it with another prompt.

We perform an extensive empirical analysis on different diffusion models to demonstrate effectiveness of our proposed attacks on the two primary semantic watermarking approaches, TreeRing [38] and Gaussian Shading [42]. A robustness and transferability analysis further shows that adjusting the detection threshold is ineffective as defense.

In summary, we make the following contributions:

- **Black-Box Attacks.** We propose two novel watermark forgery attacks that can imitate a watermark from a single watermarked reference image by only using a model that is unrelated to the watermarked model. We further introduce an adaption of the approach for watermark removal.
- **Extensive Evaluation.** We empirically show that our attacks work against two primary semantic watermarks on a range of target models, including SDXL and FLUX.1.
- **Analysis.** A thorough robustness and transferability analysis shows that simple defenses are ineffective.

## 2. Background

We start by introducing our notation and revisiting diffusion models and watermarking techniques.

### 2.1. Diffusion Models and Inverse DDIM

Diffusion models (DM) [18, 33–36] are a class of probabilistic generative models that learn a transport map between some known distribution (e.g. a standard Gaussian) and the target data distribution as the reversal of a diffusion process. During training, DMs learn a denoising function  $u(\cdot)$  that takes a noisy image  $z_t$  from an arbitrary diffusion step  $t \in \{0, \dots, T\}$  and tries to predict the noise-free version  $\hat{z}_0^t$ , which is then passed to the samplers of the diffusion process to compute a slightly less noisy version of the image,  $z_{t-1}$ . Various samplers have been proposed, with the goal to increase sampling speed [18, 21, 23, 32, 39, 45, 46] and DDIM [18] being one of the most common and straightforward sampling methods in use.

Currently, most DMs are learned in a lower-resolution latent space, which enables higher computational efficiency and leads to the name LDM. Formally, given an image  $x$ ,

an LDM uses an encoder  $\mathcal{E}$  to project  $x$  to the latent space, i.e.,  $z_0 = \mathcal{E}(x)$ , and a decoder  $D$  to project the latent presentation back to pixel space, i.e.,  $x' = D(z_0)$ . The DDIM sampler samples along a deterministic trajectory defined by the following denoising steps:

$$\hat{z}_0^t = \frac{z_t - \sqrt{1 - \alpha_t} u(z_t, t, C)}{\alpha_t}, \quad (1)$$

$$z_{t-1} = \sqrt{\alpha_{t-1}} \hat{z}_0^t + \sqrt{1 - \alpha_{t-1}} u(z_t, t, C), \quad (2)$$

where  $\alpha_t = \prod_{i=0}^t (1 - \beta_i)$  and  $\beta_t$  define the noise schedule.  $C$  is the conditioning information (e.g. textual embeddings). During generation,  $z_T$  is typically sampled from  $\mathcal{N}(\mathbf{0}, \mathbf{I})$ . We denote the full denoising process of the trained model mapping  $z_T$  back into the latent space of the auto-encoder as  $\mathcal{G}_{T \rightarrow 0}(z_T; u)$ . The full generative model is denoted as  $\Theta = (\mathcal{E}, u, D)$ .

Inverse DDIM sampling [26] tries to follow the trajectory that (would have) generated a given image in reverse. It starts from a latent image  $z_0$ , and adds noise in a step-wise fashion, where the  $t$ -th step is described by

$$z_{t+1} = \sqrt{\alpha_{t+1}} \hat{z}_0^t + \sqrt{1 - \alpha_{t+1}} u(z_t, t, C), \quad (3)$$

simply inverting the denoising steps. Note that this is different from the forward diffusion process, where random noise is added to the image. Instead, this sampler tries to follow the trajectory that generated the given image in reverse, which can be done even without knowing  $C$  [26]. We denote the inverse sampling process as  $\mathcal{I}_{0 \rightarrow T}(z_0; u)$ .

### 2.2. Watermarking

The powerful generation capabilities of diffusion models have also created an urgent need for techniques to identify and attribute images produced by these models [2, 4, 10]. In the following, we first study the use case of watermarking for generative AI and then examine watermarking approaches.

**Application.** Watermarking supports a safe and trustworthy usage of AI-generated content by enabling (1) detection and (2) attribution of generated content. **Detection** means determining whether a certain image was generated by the service provider (SP). The watermark allows the SP to claim copyright or to mark an image as AI-generated, which can be leveraged for deepfake detection. In **attribution**, the goal is to identify the user who generated a certain image using the SP. Watermarking enables the SP to identify who is violating the copyright or is distributing NSFW content.

**Watermarking methods.** Various post-processing watermarking techniques for images have been proposed [1, 9, 24, 37, 43, 48], that are applied in a post-hoc manner on existing images. Recently, watermarking methods have been developed specifically for use in large-scale text-to-image

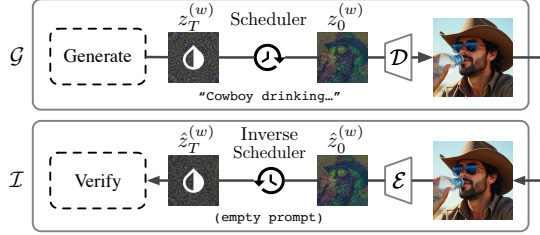


Figure 2. Concept of Semantic Watermarking. The initial latent contains a decodable watermark pattern, which can be reconstructed after inversion.

diffusion models [6, 7, 13, 38, 42]. For example, it is possible to fine-tune the decoder of an LDM to always produce watermarked images from the latents [6, 13, 40].

**Semantic Watermarking.** In this work, we focus on a specific family of watermarking methods for diffusion models that rely on the inversion of the denoising process in the diffusion model [7, 17, 38, 42]. They are easy to integrate, do not require additional training, and claim to offer significantly higher robustness to various image perturbations and targeted attacks, that earlier post-hoc-style methods (like Stable Signature [13]) are vulnerable to.

These inversion-based watermarking methods operate by modifying the initial latent  $z_T$  to have a certain structure that is recoverable using inversion and subsequently verifiable. Because only the initial latents  $z_T$  are modified, the effect of the watermark is realized as higher-level variations in the final image (as opposed to imperceptible noise patterns from post-hoc-style methods). These techniques thus drop the imperceptibility constraint from post-hoc-style methods and exploit the fact that there is a myriad of different ways to generate an image that still conforms to user specifications (e.g. the prompt). Because the watermarks are realized through higher-level image variations (such as specific details of objects and their exact arrangement), we refer to them as *semantic watermarks* [7].

Fig. 2 illustrates their general technical realization. During image generation, first a watermarked  $z_T^{(w)}$  is generated and the image is sampled as usual:  $x^{(w)} = D(\mathcal{G}_{T \rightarrow 0}(z_T^{(w)}; u))$ . In order to verify a watermark, the image is inverted ( $\hat{z}_T^{(w)} = \mathcal{I}_{0 \rightarrow T}(\mathcal{E}(x^{(w)}); u)$ ) and the watermark is extracted from  $\hat{z}_T^{(w)}$ . The different watermarking methods differ in how  $z_T^{(w)}$  is generated and verified. **Tree-Ring** [38] embeds circular patterns into the frequency representation of  $z_T^{(w)}$  and verifies the pattern by checking if the frequency representation of  $\hat{z}_T^{(w)}$  is close enough to the pattern. This method only allows the previously described detection scenario of watermarking. **Gaussian Shading** [42] takes a message bit string  $s$ , encrypts it, and uses it to select which bins of  $\mathcal{N}(0, I)$  to sample the entries of  $z_T^{(w)}$

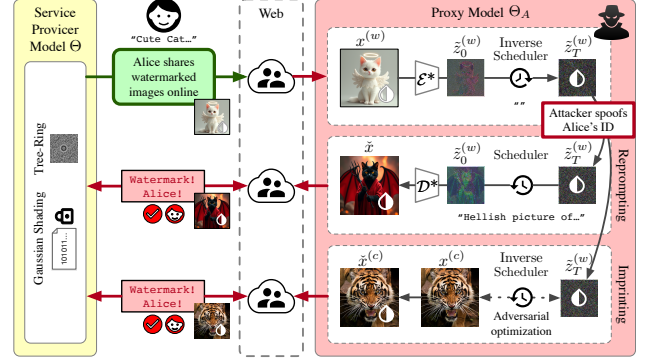


Figure 3. Illustration of our proposed watermark forgery attacks. Using a proxy model  $\Theta_A$ , the attacker first computes  $\hat{z}_0^{(w)}$  and  $\hat{z}_T^{(w)}$  (1st row). The reprompting attack (2nd row) takes  $\hat{z}_T^{(w)}$  and regenerates a novel image with another prompt. The imprinting attack (3rd row) takes an unwatermarked cover image  $x^{(c)}$  and finds a modification so that its inverted initial latent noise becomes similar to  $\hat{z}_T^{(w)}$ . Despite using  $\Theta_A$  for all computations, the attack images are verified to have the watermark from the target model.

from. The process is inverted during verification and the recovered bit string is compared to registered bit strings. Gaussian Shading allows for both detection and attribution. We describe both methods in more detail in Sec. A in the Supplementary Material. Both methods have been further improved by follow-up works [7, 17]. As the main principle relevant to our attack remains the same, we focus on the two primary approaches Tree-Ring and Gaussian Shading.

### 3. Black-Box Attacks on Semantic Watermarks

Semantic watermarks require keeping the original generative model  $\Theta$  secret—with the assumption that this prevents an attacker from forging (and removing) the watermark. In this section, however, we propose attacks that utilize a proxy model  $\Theta_A = (\mathcal{E}_A, u_A, D_A)$  for watermark forgery (and removal). In the following, we describe two forgery strategies and also discuss an adaption for watermark removal. Fig. 3 illustrates the attacks’ main principle.

#### 3.1. Watermark Imprinting Attack

Our first attack takes a clean cover image (real or generated) and slightly modifies it such that it is verified as watermarked by the SP. The procedure is as follows:

(I) The attacker takes a watermarked target image  $x^{(w)}$  that another user has generated using the SP’s model  $\Theta$ .

(II) The attacker uses the encoder  $\mathcal{E}_A$  of the proxy model to map the watermarked target image to the latent space of the attacker’s auto-encoder:  $\hat{z}_0^{(w)} = \mathcal{E}_A(x^{(w)})$ . Next, the attacker estimates the latent noise  $\hat{z}_T^{(w)}$  by running the inverse DDIM sampler  $\mathcal{I}_{0 \rightarrow T}(\hat{z}_0^{(w)}; u_A)$  of the proxy model.

(III) For a given clean cover image  $x^{(c)}$ , the attacker also computes its latent representation  $\tilde{z}_0^{(c)} = \mathcal{E}_A(x^{(c)})$ . Next, the attacker finds a difference vector  $\delta$  that decreases the Euclidean distance between  $\tilde{z}_T^{(w)}$  and the inversion of  $\tilde{z}_0^{(c)} + \delta$  by minimizing the following loss function:

$$\mathcal{L}_{\text{imprint}}(\delta) = |\mathcal{I}_{0 \rightarrow T}(\tilde{z}_0^{(c)} + \delta; u_A) - \tilde{z}_T^{(w)}|_2 \quad (4)$$

This loss is minimized by applying up to  $N$  gradient descent updates. Due to limited GPU memory, we apply gradient checkpointing to backpropagate through the entire inverse DDIM sampler. We stop when the desired watermark detection accuracy is reached. The final image  $\tilde{x}^{(c)}$  containing the stolen watermark is obtained by decoding the obtained  $(\tilde{z}_0^{(c)} + \delta)$  back to the pixel space using  $D_A$ .

(IV) When  $\tilde{x}^{(c)}$  is sent to the SP’s watermark decoding API, it gets verified as generated by the service or attributed to the user from whom  $x^{(w)}$  was collected.

Note that the inversion (Step II) and the imprinting (Step III) take place in the latent space of the proxy model  $\Theta_A$ , and do not require the target model. Still, this allows to forge the watermark from the target model, as demonstrated by our experiments in Sec. 4.

**Extension: Masking to preserve important details.** For small image sizes, certain objects such as text and human faces are susceptible to small changes in the latent variables. Simply encoding and decoding a real image with common auto-encoders already leads to noticeable distortions. In order to preserve crucial details like faces and text, we introduce a simple, yet effective extension of the procedure described above. This extension is illustrated in Fig. 4. Each gradient update on  $\delta$  uses a downsampled mask  $m_z$  to keep certain parts of the latent the same, i.e., the  $\delta$  resulting from the gradient update is replaced by  $\delta * (1 - m_z)$ . Additionally, after optimization and decoding, we paste the original pixels from  $x^{(c)}$  corresponding to the masked region to the output of the imprinting procedure  $\tilde{x}^{(c)}$  to prevent distortion introduced by the decoder  $D_A$ .

**Watermark Removal.** It is also possible to remove watermarks using the same methodology. In the removal set-up, instead of a cover image, we have the same watermarked image  $x^{(w)}$  that we aim to modify so that it no longer contains its original watermark. To accomplish this, we simply change the target  $\tilde{z}_T^{(w)}$  in Eq. (4) to its negation  $-\tilde{z}_T^{(w)}$  (Step III). This leads to the following loss, which encourages erasing the watermark pattern encoded in the initial latent noise of the watermarked image:

$$\mathcal{L}_{\text{imprint}}(\delta) = |\mathcal{I}_{0 \rightarrow T}(\tilde{z}_0^{(w)} + \delta; u_A) + \tilde{z}_T^{(w)}|_2 \quad (5)$$

Images obtained through this procedure should no longer verify as watermarked.

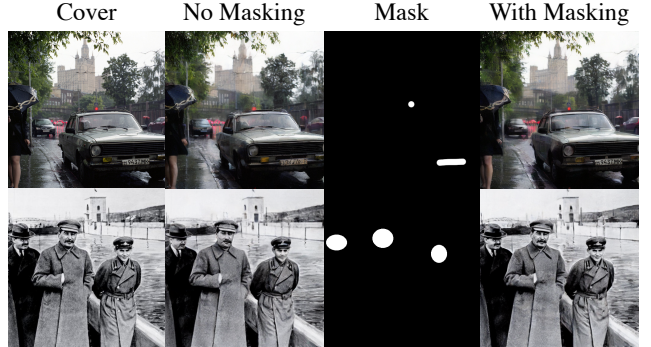


Figure 4. Imprinting attack with and without masking. Masking is a way to preserve crucial details that are distorted by the auto-encoder, such as text and faces. The attacks are performed using SD2.1 as proxy model, against an image of size  $512 \times 512$  generated by FLUX.1-dev with Gaussian Shading watermarking.

### 3.2. Watermark Reprompting Attack

Our second attack strategy aims at generating new (potentially harmful) images that are verified to have the target watermark. To this end, we replace Step III of the previously described imprinting attack. Starting from the extracted  $\tilde{z}_T^{(w)}$ , the attacker just generates a different image  $\tilde{x}$  with the desired target prompt using the proxy model  $\Theta_A$ .

**Multiple Prompts and Bin Resampling.** To improve the attack effectiveness, we propose two simple, yet effective augmentations. First, the attacker can try multiple prompts (all of which may prompt for harmful content). Second, for Gaussian Shading, the attacker can also resample  $\tilde{z}_T^{(w)}$  such that the values in  $\tilde{z}_T^{(w)}$  remain in the same bin. In the default setup of Gaussian Shading, it means each value must retain its sign. This procedure preserves the encoded watermark in  $\tilde{z}_T^{(w)}$ , but provides a novel seed for the diffusion process.

## 4. Evaluation

We proceed with an empirical evaluation to demonstrate the effectiveness of the proposed attacks.

### 4.1. Experimental Setting

We use Stable Diffusion 2.1 [30] as attacker model and evaluate several common models as target model, namely Stable Diffusion XL (SDXL) [28], PixArt- $\Sigma$  [5] and FLUX.1. We also include our own finetune of SD2.1 trained on anime (SD2.1-Anime). All experiments use  $512 \times 512$  images.

We evaluate the two primary semantic watermarking approaches: Tree-Ring [38] and Gaussian Shading [42]. To ensure consistency with their respective experimental setups, we consider the same scenarios and metrics. As Tree-Ring operates only in the detection scenario, we measure the watermark detection rate using the TPR@1%FPR. The underlying

Model	Step	Gaussian Shading (FPR= $10^{-6}$ )			Tree-Ring (FPR= $10^{-2}$ )	
		Det.	Attr.	PSNR	Det.	PSNR
SD2.1-Anime	50	1.00	1.00	30.35	1.00	30.35
	100	1.00	1.00	30.00	1.00	29.99
	150	1.00	1.00	29.78	1.00	29.77
SDXL	50	1.00	1.00	30.31	0.72	30.32
	100	1.00	1.00	29.98	0.95	29.97
	150	1.00	1.00	29.78	0.99	29.77
PixArt- $\Sigma$	50	0.91	0.91	30.35	0.55	30.34
	100	0.94	0.94	30.00	0.78	29.99
	150	0.96	0.96	29.78	0.84	29.78
FLUX.1	50	0.66	0.66	30.49	0.13	30.42
	100	0.88	0.88	30.14	0.20	30.08
	150	0.95	0.95	29.92	0.28	29.87

Table 1. Imprinting Attack against Gaussian Shading and Tree-Ring applied on different target models. The attacker uses a vanilla SD 2.1 model as proxy. Watermark detection (“Det.”) and user attribution (“Attr.”) success are measured using TPR@ $X$ -FPR. We use PSNR to measure deviation from the original images.

threshold for detecting an image as watermarked is based on the p-value, which reflects the likelihood of observing the watermark pattern by random chance. Gaussian Shading is evaluated for detection and attribution. To this end, the raw bit accuracy  $r(s, s')$  is used to measure how many bits of the recovered message bit string  $s'$  from an image under investigation match with the bit string  $s$  from the target watermark. In the detection scenario, we count a true positive if  $r(s, s')$  exceeds a threshold  $\tau$  which in turn is calibrated to achieve a specific FPR<sup>1</sup>. For attribution, we compute  $r(s, s')$  between the recovered bit string  $s'$  from an image under investigation belonging to a target user and each bit string  $s$  from a pool of 100k users. Like Yang et al. [42], we count a true positive as follows. First, the user id with the highest number of matching bits is retrieved. Then, if the number of matching bits exceeds the threshold  $\tau$  corresponding to a FPR of  $10^{-6}$ , the sample is counted if attributed to the correct target user.

We encourage the reader to consult Sec. B in the Supplementary Material for visual results, as well as Sec. C for more details on prompt and image datasets, exact parameters of model settings and threshold computations.

## 4.2. Imprinting Attack for Forgery

In our first experiment, we investigate whether an attacker can imprint a semantic watermark on existing images by using our proposed imprinting attack. For pairs of 100 watermarked images and natural cover images, we minimize Eq. (4) for 150 steps with a learning rate of 0.01, and evalu-

<sup>1</sup>Following Yang et al. [42], we calculate the FPR for a threshold based on the probability of generating the correct bit sequence by random chance.

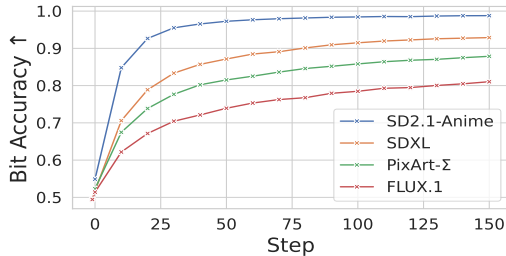


Figure 5. Bit accuracy for Gaussian Shading imprinting at different optimization steps. Attacker aims at higher values.

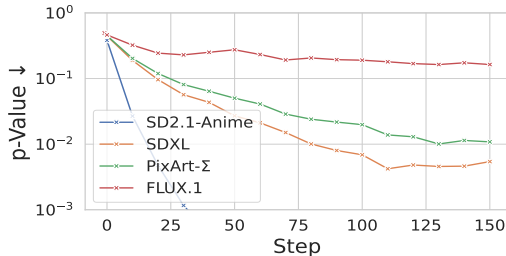


Figure 6. P-values for Tree-Ring imprinting at different optimization steps. Attacker aims at smaller values.

ate at every tenth step. As we outline in Sec. 5, there are no suitable baselines for comparison.

**Results.** Tab. 1 presents the performance of the attack against both watermarking methods. For Gaussian Shading, the attack successfully implants a watermark that is detected in almost all images across different models in the detection and the attribution scenarios. For Tree-Ring, the attack achieves more than 84% detection rate for three out of four models. In all cases, the attacks retain overall picture content and quality (see PSNR in Tab. 1, qualitative examples in Fig. 4, and Sec. B in Supplementary Material).

We account the lower success rate for Tree-Rings on FLUX.1 to the fact that Tree-Ring embeds a weaker watermark signal than Gaussian Shading while FLUX.1 is a completely unrelated model with a different architecture and auto-encoder. This makes successful transfer more difficult. Still, almost 30% are attributed, which is still enough to discredit the watermarking method. Regarding the number of optimization steps, we find that 50 steps are often enough to successfully imprint a watermark in the cover image.

Figs. 5 and 6 show the evolution of the bit accuracies and p-values as optimization progresses. From the plots, we can see clear trends towards higher bit accuracies and lower p-values. We can also clearly see the different degrees of transferability, where more similar models (SD2.1-Anime) can be attacked much more easily.

## 4.3. Imprinting Attack for Removal

In our next experiment, we test the effectiveness of the proposed watermark removal technique. We optimize Eq. (5) for

Model	Attk	Step	Gaussian Shading (FPR=10 <sup>-6</sup> )			Tree-Ring (FPR=10 <sup>-2</sup> )	
			Det.	Attr.	PSNR	Det.	PSNR
SD2.1-Anime	AdvE	200	1.00	1.00	31.30	0.94	31.27
	Ours	50	0.00	0.00	31.08	0.14	31.12
		100	0.00	0.00	30.49	0.04	30.45
		150	0.00	0.00	30.12	0.03	30.02
SDXL	AdvE	200	1.00	1.00	31.33	0.99	31.41
	Ours	50	0.00	0.00	30.42	0.64	30.89
		100	0.00	0.00	29.90	0.33	30.22
		150	0.00	0.00	29.65	0.12	29.90
PixArt- $\Sigma$	AdvE	200	1.00	1.00	31.53	0.93	31.48
	Ours	50	0.18	0.18	31.14	0.75	31.22
		100	0.00	0.00	30.49	0.41	30.49
		150	0.00	0.00	30.14	0.14	30.10
FLUX.1	AdvE	200	1.00	1.00	31.33	0.64	31.43
	Ours	50	0.00	0.00	30.14	0.00	30.55
		100	0.00	0.00	29.59	0.00	30.00
		150	0.00	0.00	29.28	0.00	29.69

Table 2. Our removal attack and AdvEmb baseline (AdvE) against Gaussian Shading and Tree-Ring. The same target models and metrics from the imprinting experiments (see Tab. 1) are used here. Note, however, that attack success for removal is assessed by the decrease in detection and attribution metrics.

150 steps with a learning rate of 0.01 for 100 watermarked images, and evaluate at every tenth step.

As baseline, we also include the similar adversarial embedding (AdvEmb) attack [29]. It performs PGD to move away from the initial image in latent space while staying within a perturbation budget  $\epsilon$  in pixel space:  $\max_{x_{adv}} \|\mathcal{E}_A(x_{adv}) - \mathcal{E}_A(x^{(w)})\|_2$  s.t.  $\|x_{adv} - x^{(w)}\|_\infty \leq \epsilon$ . We use their implementation, set  $\epsilon = 8/255$ , and otherwise use the default parameters, such as 200 optimization steps. Again, the auto-encoder of SD2.1 is used for the attack, which corresponds to their black-box setting.

**Results.** Tab. 2 shows the results for the removal attack. For Gaussian Shading, after 100 steps, watermarks are no longer detectable in either the detection or attribution setting. Removal of Tree-Ring watermarks is more challenging but TPR@1%FPR eventually drops below 15% for all target models. In Figs. 7 and 8, we observe similar trends in transferability as seen for imprinting. An exception is FLUX.1, which shows an immediate sharp increase in the p-values. This is likely caused by significant auto-encoder differences with SD2.1.

Compared to the baseline attack (AdvEmb), our removal attack is clearly more effective. The baseline also introduces distracting patterns, which are very noticeable even before their removal success reaches an acceptable level.

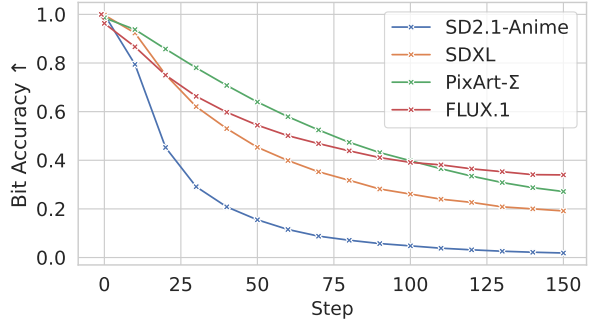


Figure 7. Bit accuracy of removal attack against Gaussian Shading at different optimization steps. Attacker aims at smaller values.

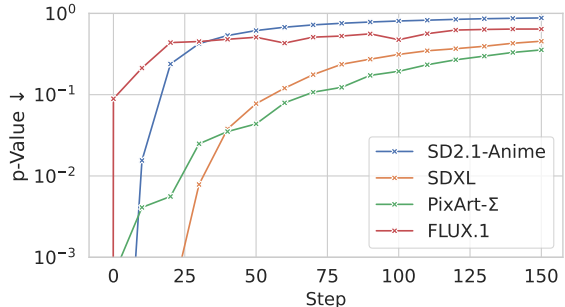


Figure 8. P-values of removal attack against Tree-Ring at different optimization steps. Attacker aims at higher values.

#### 4.4. Reprompting Attack

In this experiment, we evaluate the effectiveness of our re-prompting forgery attack. As outlined in Sec. 3.2, we have a basic variant which re-generates an image on  $\Theta_A$  with another prompt, and an augmented variant that tries  $k$  prompts, and for Gaussian Shading  $l$  bin resamplings in addition. For the basic variant (“Attk”), for each target model, we use 1000 watermarked images and re-generate an attack image using a harmful prompt. For the augmented variant (“Attk+”), for each target model, we use 100 target images and set  $k = 3$  and  $l = 3$ . That is, we have 3 attack candidates for each target image with Tree-Ring, and 9 attack candidates with Gaussian Shading. If the watermark is valid in one of the candidates, we count the target image as successfully forged.

**Results.** Tab. 3 depicts the attack performance. Both watermarking methods can be successfully tricked. With Gaussian Shading, the attack achieves a near-perfect detection and identification rate on all models. With Tree-Ring, three out of four models detect the forged watermark in almost all cases. Similar to the imprinting attack, FLUX.1 is harder to attack; however, 35% of the images are still detected as watermarked which is enough to undermine the method. Comparing the two attack variants, even the basic variant achieves a high success rate in different settings, which can often be increased to (almost) 100% using the augmented variant.

Model		G. Shad. (FPR= $10^{-6}$ )		Tree-Ring (FPR= $10^{-2}$ )
		Det.	Attr.	Det.
SD2.1-Anime	Attk	0.983	0.983	0.896
	Attk+	1.000	1.000	1.000
SDXL	Attk	0.995	0.995	0.968
	Attk+	1.000	1.000	1.000
PixArt- $\Sigma$	Attk	0.934	0.934	0.875
	Attk+	1.000	1.000	0.990
FLUX.1	Attk	0.656	0.656	0.128
	Attk+	0.880	0.880	0.350

Table 3. Detection TPR (“Det.”) and attribution accuracy (“Attr.”) for the reprompting attack. The metrics are computed as in the imprinting experiments (see Tab. 1). *Attk* is the default reprompting attack, *Attk+* is the enhanced reprompting attack.

#### 4.5. Transferability Analysis

The previous experiments show the effectiveness of our proposed attacks. In the next step, we further analyze the transferability across different models to understand the extent to which models are vulnerable. To this end, we examine our reprompting attack in the basic variant across different pairs of target and attacker model. In addition to SD2.1, SDXL and PixArt- $\Sigma$ , we include SD1.5, Mitsua Diffusion One, Common Canvas S-C [14] and Waifu Diffusion. We consider Mitsua and Common Canvas as they share the same architecture as Stable Diffusion models but are trained from scratch on different datasets. Waifu Diffusion is an extensive community fine-tune of SD1.4. Additional information on these models are provided in Sec. C in the Supplementary Material. For each target model, we use 100 watermarked images from this model to create respective forgeries on the attacker model.

**Results.** Fig. 10 illustrates the transferability in terms of bit accuracy (Gaussian Shading) and p-value (Tree-Ring). Similar models (SD1.5, SD2.1) and their fine-tunes (Waifu) show nearly-100% bit accuracy and extremely low p-values across all combinations. When considering models that have been trained independently *from scratch* (Mitsua, Common Canvas) on public domain data but have a similar architecture, we also observe a high transferability. Thus, even models with different training data and possible different training protocols are severely impacted by our attack.

**Analysis.** We continue by analyzing the unexpected transferability of inversion that enables our attacks. We find a correlation between the success of attacks on different target and proxy models and the functional similarity of their corresponding auto-encoders. This indicates that our attacks benefit from high similarity in the latent spaces between

target and proxy models. We encourage readers to consult Sec. D in the Supplementary Material for more details.

#### 4.6. No Defense by Adjusting Thresholds

Finally, we demonstrate that a defender cannot simply make the thresholds in the watermarking method tighter, that is, a lower p-value for Tree-Ring and a higher bit accuracy for Gaussian Shading. The first problem is that a watermark must be resilient to common perturbations, such as JPEG compression and Gaussian Noise, to be practical. This requirement significantly limits the feasible thresholds. The second problem is that our attack images achieve p-values and bit accuracies that already overlap with those of the original, unperturbed watermarked images.

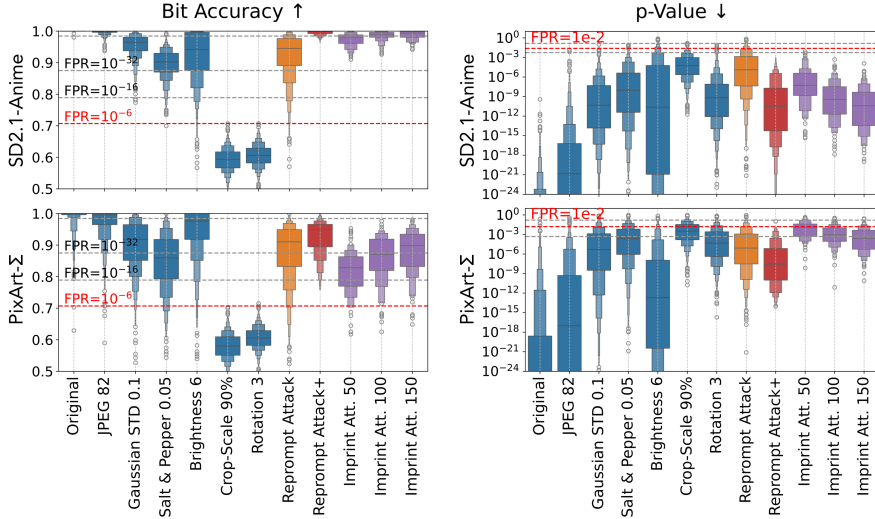
**Setup.** We adopt the attack setup as outlined in previous sections, and report results for SD2.1-Anime and PixArt- $\Sigma$  as target models. We consider the standard perturbations from related work that are applied to watermarked images before watermark verification: JPEG compression (82 quality), Gaussian Noise ( $\sigma=0.1$ ), Salt-and-Pepper noise ( $p=0.05$ ), brightness jitter, Rotation (3 degrees), 90% crop-and-scale. We measure the p-value for Tree-Ring and the bit accuracy for Gaussian Shading on watermarked images that have undergone one of these perturbations, and on attack images from our different forgery attacks. We provide examples of the transformations in Sec. C in the Supplementary Material.

**Results.** Fig. 9 depicts the measured p-values for Tree-Ring and bit accuracies for Gaussian Shading across different input types. It is not possible to tighten the detection threshold enough to distinguish attack images (orange, red and purple bars) while maintaining robustness to common perturbations (blue bars). For example, salt-and-pepper noise results in higher p-values for Tree-Ring and lower bit-accuracies for Gaussian Shading, which are comparable to those of our attack images. We can conclude that tightening thresholds is not a viable defense.

### 5. Related Work

In the following, we recap related work that examines security aspects of inversion-based semantic watermarks.

**Forgery Attacks.** There is little prior work on the forgery of semantic watermarks. These works focus on Tree-Ring and operate on unrealistic assumptions. Saberi et al. [31] propose a method against Tree-Ring where the attacker requests the SP to generate a white-noise image containing a watermark, and then blends this image into a clean cover image. However, obtaining white-noise images from a black-box API through prompting is challenging and easy to defend against. In their code implementation, this is realized by having the SP artificially sample white-noise pixels, applying DDIM inversion, embedding a Tree-Ring, and regenerating the image. Furthermore, the attack does not work for watermarks



(a) Bit Accuracy ( $\uparrow$ ) for Gaussian Shading on SD2.1-Anime (top) and PixArt- $\Sigma$  (bottom). (b) P-values ( $\downarrow$ ) for Tree-Ring on SD2.1-Anime (top) and PixArt- $\Sigma$  (bottom).

Figure 9. Impact of common transformations (blue) and our forgery attacks (orange, red, purple) on bit accuracy and p-values, and thus on suitable thresholds for watermarking. No threshold can effectively separate images from common transformations and attacks.

that do attribution. As the attacker requests watermarked images from the SP, all forged images are traceable to the attacker. Yang et al. [41] propose to average watermarked images—either in the pixel space or their inverted latents—to get a watermark pattern which is then added on clean cover images (or removed from watermarked images). This attack, however, requires access to the original model for the inversion or a large number of watermarked images if working in the pixel space. Neither is the attack applicable against Gaussian Shading, which draws a unique watermark key for each image.

In contrast, our forgery attacks work with just a single watermarked image, are applicable under detection and attribution, and work for Tree-Ring and Gaussian Shading. Access to the target watermarked model is not needed either.

**Removal Attacks.** The removal of semantic watermarks, and more specifically of tree-ring watermarks, has been studied in several works. Concurrently to our work, Liu et al. [22] proposes a method based on controllable regeneration from clean noise. They train a special adapter for semantic control and use a ControlNet [44] for spatial control. In contrast, the methods presented in this work are completely training-free and instead rely on cleaning the initial latent using gradient descent. Simpler regeneration attacks have also been studied in recent work on watermark removal [29, 47], but were found ineffective for semantic watermark removal [47]. Zhao et al. [47] remove watermarks by applying noise and regenerating using diffusion models. Lukas et al. [25] and Yang et al. [41] are able to learn a Tree-Ring key and use it

for watermark removal. However, their approaches require multiple examples for training. Similarly, surrogate-detector methods [29, 31] also require training on multiple examples and would fail against learning the random distribution of initial latents produced with Gaussian Shading.

## 6. Discussion and Conclusion

The attacks described in this paper expose fundamental issues in the practical use of current inversion-based semantic watermarking approaches. In a realistic scenario, where the attacker can simply leverage their own model, we show that the attacker can forge and remove semantic watermarks with almost perfect success rate. Concerningly, even a large difference between the attacker and the target watermarked model still permits an attack, as the high attack success rates on completely unrelated and independently trained target models show. For instance, our attacks succeed even when the attacker uses an SD2.1 model against PixArt- $\Sigma$  and FLUX.1, which are both DiT [27] models trained from scratch.

From a defense perspective, we find that adjusting the watermark detection thresholds is not effective. We believe that fundamental improvements of semantic watermarking techniques are required to prevent watermarks from being easily imposed on new images. Another avenue of future work is the development of semantic watermarks that do not rely on inversion, similarly to the work of Feng et al. [12].

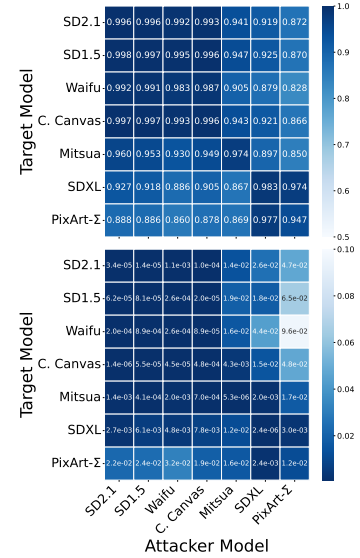


Figure 10. Transferability in terms of bit accuracy (Gaussian Shading, top) and p-value (Tree-Ring, bottom) of the reprompting attack across models.



## Acknowledgements

This work was funded by the Deutsche Forschungsgemeinschaft (DFG, German Research Foundation) under Germany’s Excellence Strategy – EXC 2092 CASA – 390781972.

## References

- [1] A. Al-Haj. Combined dwt-dct digital image watermarking. *Journal of computer science*, 3(9):740–746, 2007. 2
- [2] D. Bartz and K. Hu. Openai, google, others pledge to watermark ai content for safety, white house says. <https://www.reuters.com/technology/openai-google-others-pledge-watermark-ai-content-safety-white-house-2023-07-21/>, 2023. 1, 2
- [3] D. J. Bernstein et al. Chacha, a variant of salsa20. In *Workshop record of SASC*, volume 8, pages 3–5. Citeseer, 2008. 11
- [4] J. R. Biden. Executive order on the safe, secure, and trustworthy development and use of artificial intelligence. <https://www.whitehouse.gov/briefing-room/presidential-actions/2023/10/30/executive-order-on-the-safe-secure-and-trustworthy-development-and-use-of-artificial-intelligence/>, 2023. 2
- [5] J. Chen, J. Yu, C. Ge, L. Yao, E. Xie, Y. Wu, Z. Wang, J. Kwok, P. Luo, H. Lu, and Z. Li. Pixart- $\alpha$ : Fast training of diffusion transformer for photorealistic text-to-image synthesis. arXiv:2310.00426, 2023. 4
- [6] H. Ci, Y. Song, P. Yang, J. Xie, and M. Z. Shou. Wmadapter: Adding watermark control to latent diffusion models. arXiv:2406.08337, 2024. 3
- [7] H. Ci, P. Yang, Y. Song, and M. Z. Shou. Ringid: Rethinking tree-ring watermarking for enhanced multi-key identification. arXiv:2404.14055, 2024. 1, 3, 11
- [8] N. Clegg. Labeling AI-Generated images on Facebook, Instagram and Threads. <https://about.fb.com/news/2024/02/labeling-ai-generated-images-on-facebook-instagram-and-threads/>, 2024. 1
- [9] I. Cox, M. Miller, J. Bloom, J. Fridrich, and T. Kalker. *Digital Watermarking and Steganography*. Morgan Kaufmann Publishers Inc., San Francisco, CA, USA, 2 edition, 2007. 2
- [10] European Union. Artificial intelligence act: Regulation (EU) 2024/1689 of the european parliament and of the council, 2024. <https://eur-lex.europa.eu/legal-content/EN/TXT/?uri=CELEX:32024R1689>. 2
- [11] Europol Innovation Lab. Facing reality? law enforcement and the challenge of deepfakes. <https://www.europol.europa.eu/publications-events/publications/facing-reality-law-enforcement-and-challenge-of-deepfakes>, 2024. 1
- [12] W. Feng, W. Zhou, J. He, J. Zhang, T. Wei, G. Li, T. Zhang, W. Zhang, and N. Yu. AqualoRA: Toward white-box protection for customized stable diffusion models via watermark loRA. In *Proc. of Int. Conference on Machine Learning (ICML)*, 2024. 8
- [13] P. Fernandez, G. Couairon, H. Jégou, M. Douze, and T. Furon. The stable signature: Rooting watermarks in latent diffusion models. In *Proc. of IEEE Conference on Computer Vision and Pattern Recognition (CVPR)*, 2023. 3
- [14] A. Gokaslan, A. F. Cooper, J. Collins, L. Seguin, A. Jacobson, M. Patel, J. Frankle, C. Stephenson, and V. Kuleshov. Commoncanvas: An open diffusion model trained with creative-commons images. arXiv:2310.16825, 2023. 7
- [15] J. A. Goldstein and S. Grossman. How disinformation evolved in 2020, 2021. 1
- [16] Google DeepMind. SynthID: Identifying ai-generated content with SynthID. <https://deepmind.google/technologies/synthid/>, Last visit: Nov. 2024. 1
- [17] S. Gunn, X. Zhao, and D. Song. An undetectable watermark for generative image models. arXiv:2410.07369, 2024. 1, 3
- [18] J. Ho, A. Jain, and P. Abbeel. Denoising diffusion probabilistic models. In *Advances in Neural Information Processing Systems*, 2020. 2
- [19] Hugging Face / Diffusers. Stable diffusion XL repository. [https://github.com/huggingface/diffusers/blob/main/src/diffusers/pipelines/stable\\_diffusion\\_xl/pipeline\\_stable\\_diffusion\\_xl.py](https://github.com/huggingface/diffusers/blob/main/src/diffusers/pipelines/stable_diffusion_xl/pipeline_stable_diffusion_xl.py), Last visit: Nov. 2024. 1
- [20] T.-Y. Lin, M. Maire, S. Belongie, J. Hays, P. Perona, D. Ramanan, P. Dollár, and C. L. Zitnick. Microsoft coco: Common objects in context. In *Computer Vision–ECCV 2014: 13th European Conference, Zurich, Switzerland, September 6–12, 2014, Proceedings, Part V 13*, 2014. 18, 21
- [21] L. Liu, Y. Ren, Z. Lin, and Z. Zhao. Pseudo numerical methods for diffusion models on manifolds. In *International Conference on Learning Representations (ICLR)*, 2022. 2
- [22] Y. Liu, Y. Song, H. Ci, Y. Zhang, H. Wang, M. Z. Shou, and Y. Bu. Image watermarks are removable using controllable regeneration from clean noise. arXiv:2410.05470, 2024. 8
- [23] C. Lu, Y. Zhou, F. Bao, J. Chen, C. Li, and J. Zhu. DPM-solver: A fast ODE solver for diffusion probabilistic model sampling in around 10 steps. In *Advances in Neural Information Processing Systems (NeurIPS)*, 2022. 2
- [24] S. Lu, Z. Zhou, J. Lu, Y. Zhu, and A. W.-K. Kong. Robust watermarking using generative priors against image editing: From benchmarking to advances. arXiv:2410.18775, 2024. 2
- [25] N. Lukas, A. Diaa, L. Fenaux, and F. Kerschbaum. Leveraging optimization for adaptive attacks on image watermarks. In *The Twelfth International Conference on Learning Representations*, 2024. 8
- [26] R. Mokady, A. Hertz, K. Aberman, Y. Pritch, and D. Cohen-Or. Null-text inversion for editing real images using guided diffusion models. In *Proc. of IEEE Conference on Computer Vision and Pattern Recognition (CVPR)*, 2023. 2
- [27] W. Peebles and S. Xie. Scalable diffusion models with transformers. In *Proceedings of the IEEE/CVF International Conference on Computer Vision (ICCV)*, 2023. 8
- [28] D. Podell, Z. English, K. Lacey, A. Blattmann, T. Dockhorn, J. Müller, J. Penna, and R. Rombach. SDXL: Improving latent diffusion models for high-resolution image synthesis. In *International Conference on Learning Representations (ICLR)*, 2024. 4

- [29] T. Rabbani, B. An, M. Ding, A. Agrawal, Y. Xu, C. Deng, S. Zhu, A. Mohamed, Y. Wen, T. Goldstein, and F. Huang. WAVES: Benchmarking the robustness of image watermarks. In *Privacy Regulation and Protection in Machine Learning*, 2024. 6, 8, 17
- [30] R. Rombach, A. Blattmann, D. Lorenz, P. Esser, and B. Ommer. High-resolution image synthesis with latent diffusion models. In *Proceedings of the IEEE/CVF Conference on Computer Vision and Pattern Recognition (CVPR)*, 2022. 4
- [31] M. Saberi, V. S. Sadasivan, K. Rezaei, A. Kumar, A. M. Chegini, W. Wang, and S. Feizi. Robustness of ai-image detectors: Fundamental limits and practical attacks. In *The Twelfth International Conference on Learning Representations, ICLR 2024, Vienna, Austria, May 7-11, 2024*. OpenReview.net, 2024. 7, 8
- [32] T. Salimans and J. Ho. Progressive distillation for fast sampling of diffusion models. In *International Conference on Learning Representations (ICLR)*, 2022. 2
- [33] J. Sohl-Dickstein, E. Weiss, N. Maheswaranathan, and S. Ganguli. Deep unsupervised learning using nonequilibrium thermodynamics. In *Proc. of Int. Conference on Machine Learning (ICML)*, 2015. 2
- [34] J. Song, C. Meng, and S. Ermon. Denoising diffusion implicit models. In *International Conference on Learning Representations (ICLR)*, 2021.
- [35] Y. Song and S. Ermon. *Generative modeling by estimating gradients of the data distribution*. Curran Associates Inc., 2019.
- [36] Y. Song, J. Sohl-Dickstein, D. P. Kingma, A. Kumar, S. Ermon, and B. Poole. Score-based generative modeling through stochastic differential equations. In *International Conference on Learning Representations (ICLR)*, 2021. 2
- [37] M. Tancik, B. Mildenhall, and R. Ng. Stegastamp: Invisible hyperlinks in physical photographs. In *Proceedings of the IEEE/CVF conference on computer vision and pattern recognition*, pages 2117–2126, 2020. 2
- [38] Y. Wen, J. Kirchenbauer, J. Geiping, and T. Goldstein. Tree-rings watermarks: Invisible fingerprints for diffusion images. In *Advances in Neural Information Processing Systems (NeurIPS)*, 2023. 1, 2, 3, 4, 11, 19
- [39] Z. Xiao, K. Kreis, and A. Vahdat. Tackling the generative learning trilemma with denoising diffusion GANs. In *International Conference on Learning Representations (ICLR)*, 2022. 2
- [40] C. Xiong, C. Qin, G. Feng, and X. Zhang. Flexible and secure watermarking for latent diffusion model. In *Proceedings of the 31st ACM International Conference on Multimedia*, 2023. 3
- [41] P. Yang, H. Ci, Y. Song, and M. Z. Shou. Steganalysis on digital watermarking: Is your defense truly impervious? arXiv:2406.09026, 2024. 8
- [42] Z. Yang, K. Zeng, K. Chen, H. Fang, W. Zhang, and N. Yu. Gaussian shading: Provable performance-lossless image watermarking for diffusion models. In *Proc. of IEEE Conference on Computer Vision and Pattern Recognition (CVPR)*, 2024. 1, 2, 3, 4, 5, 11, 12, 20
- [43] K. A. Zhang, L. Xu, A. Cuesta-Infante, and K. Veeramachani. Robust invisible video watermarking with attention. arXiv:1909.01285, 2019. 2
- [44] L. Zhang, A. Rao, and M. Agrawala. Adding conditional control to text-to-image diffusion models. In *Proc. of IEEE Conference on Computer Vision and Pattern Recognition (CVPR)*, 2023. 8
- [45] Q. Zhang and Y. Chen. Fast sampling of diffusion models with exponential integrator. In *International Conference on Learning Representations (ICLR)*, 2023. 2
- [46] W. Zhao, L. Bai, Y. Rao, J. Zhou, and J. Lu. UniPC: A unified predictor-corrector framework for fast sampling of diffusion models. In *Advances in Neural Information Processing Systems (NeurIPS)*, 2023. 2
- [47] X. Zhao, K. Zhang, Z. Su, S. Vasani, I. Grishchenko, C. Kruegel, G. Vigna, Y.-X. Wang, and L. Li. Invisible image watermarks are provably removable using generative AI. In *Advances in Neural Information Processing Systems (NeurIPS)*, 2024. 8
- [48] J. Zhu, R. Kaplan, J. Johnson, and L. Fei-Fei. Hidden: Hiding data with deep networks. In *Proceedings of the European Conference on Computer Vision (ECCV)*, 2018. 2

# Supplementary Material

## A. Semantic Watermarking

In this section, we present more details on the examined semantic watermarking methods.

**Tree-Ring.** Wen et al. [38] have initially presented the concept of inversion-based semantic watermarking. Fig. 11a illustrates the proposed Tree-Ring watermark approach, which can be divided into two phases.

- *Generation.* During image generation, Tree-Ring modifies a clean initial latent  $z_T \sim \mathcal{N}(\mathbf{O}, \mathbf{I})$  by adding a concentric circular pattern into its frequency representation. This step produces the watermarked latent noise  $z_T^{(w)}$ . This noise vector is then used as usual in the further generation process (denoising + decoding) to finally obtain the watermarked image:  $x^{(w)} = D(\mathcal{G}_{T \rightarrow 0}(z_T^{(w)}; u))$ .
- *Verification.* The inverse  $\hat{z}_T^{(w)} = \mathcal{I}_{0 \rightarrow T}(\mathcal{E}(x^{(w)}); u)$  is computed, and then the existence of the original circular pattern in the frequency spectrum of  $\hat{z}_T^{(w)}$  is checked. The final detection is based on a statistical test. The test statistic aggregates the squared absolute difference between the observed and the expected frequency values from each respective ring. The null hypothesis  $H_0$  is that an input image is not watermarked. In this case, its inverted initial latent noise should follow a Gaussian distribution with an unknown variance. Under  $H_0$ , the test statistic leads to a noncentral  $\chi^2$  distribution. This allows computing a p-value that reflects the probability of observing the test-statistic output under the assumption that the input image is not watermarked. If the p-value is below a pre-defined threshold  $\tau$ ,  $H_0$  is rejected and the watermark’s presence is assumed.

Tree-Ring is designed as a so-called zero-bit watermarking scheme, as only watermark presence or absence can be detected. Note that the modification to the sampling procedure changes which images will be generated (it is not distribution-preserving), but appears to still have sufficient variety in generated images while retaining image quality.

A subsequent work, RingID [7], improves Tree-Ring by making it more robust to perturbations, ensuring that the distribution of  $z_T^{(w)}$  is closer to  $\mathcal{N}(\mathbf{O}, \mathbf{I})$ , and providing so-called multi-bit watermarking which can carry a multiple bit long message and thus allows distinguishing between different users.

**Gaussian Shading.** Yang et al. [42] expand the previous concept by relying on cryptographic primitives to achieve distribution-preserving generation. Fig. 11b illustrates the two phases of Gaussian Shading:

- *Generation.* A message  $s$  of length  $k$  is created. This message  $s$  is first repeated (“diffused”)  $\rho$  times to obtain  $s^d$ , which is then encrypted using the symmetric stream cipher ChaCha20 [3]. This stream cipher takes a secret key and a random seed as input, which are completely random for each image. The encrypted message  $m$  is then used to steer the sampling of  $z_T^{(w)}$ . To this end, Gaussian Shading splits a Gaussian distribution into  $2^\ell$  bins with equal probability. In the following, we focus on the standard setting with  $\ell = 1$ . This means we have two bins, the negative and the positive area of the Gaussian curve. The bit in the encrypted message  $m[i] \in \{0, 1\}$  specifies if  $z_T^{(w)}[i]$  is sampled from the negative or the positive area of a Gaussian distribution. Due to the encryption, the bits in  $m$  are uniformly distributed, ensuring a similar number of positive and negative samples from the Gaussian distribution. Hence,  $z_T^{(w)}$  still follows a Gaussian distribution. After this sampling step, the usual generation process continues with  $x^{(w)} = D(\mathcal{G}_{T \rightarrow 0}(z_T^{(w)}; u))$ .

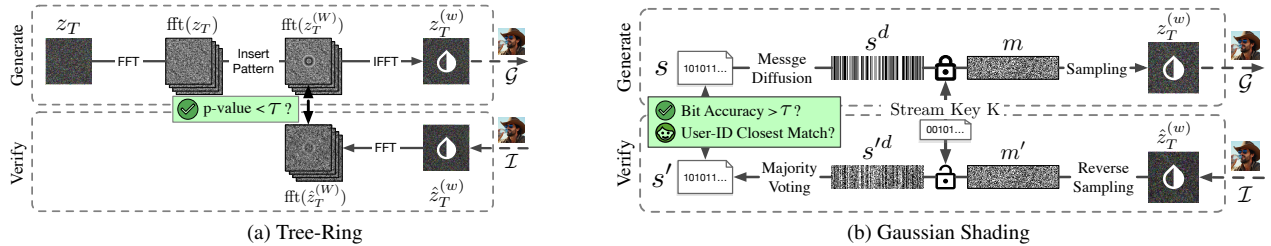


Figure 11. Concept of the two inversion-based semantic watermarking approaches

- *Verification.* To verify the watermark, Gaussian Shading also relies on a full inversion using  $\mathcal{I}_{0 \rightarrow T}(\hat{z}_0^{(w)}; u)$  to obtain an estimated  $\hat{z}_T^{(w)}$ . This inverted latent noise  $\hat{z}_T^{(w)}$  is quantized to retrieve encrypted message bits  $m'$ , that is, we assume  $m'[i] = 0$  if  $\hat{z}_T^{(w)}[i] < 0$  and  $m'[i] = 1$  if  $\hat{z}_T^{(w)}[i] \geq 0$ . Next,  $m'$  is decrypted to reconstruct the message  $s'^d$ . Since each bit was repeated  $\rho$  times, its value is recovered by performing a majority voting on all its duplicates to finally obtain  $s'$ . This step corrects errors and makes the scheme more robust to noise.

Gaussian Shading is applicable for both zero-bit watermarking and multi-bit watermarking. In both cases,  $s'$  is compared to some  $s$  bit-wise and the number of matches per message length is recorded as bit-accuracy  $r(s, s')$ . Like Tree-Ring, a statistical test is performed, but this time the distribution is assumed to be binomial if the image is not watermarked and therefore the test is computed using a regularized incomplete beta function. In zero-bit watermarking,  $s'$  is compared to the predefined message  $s$  used by the SP. It is checked if a certain fraction of at least  $\tau$  % of the bits match, such that it is unlikely to observe this by chance with a predefined FPR, which is denoted as  $\text{FPR}(\tau)$ . In multi-bit watermarking,  $s'$  is a specific user id. It is compared with all user ids known to the SP. The match with the best accuracy  $r(s, s')$  is selected and then checked if the value is above the threshold  $\tau$ . As this resembles a multiple test, in order to maintain a certain FPR, the threshold  $\tau$  is adapted depending on the number of users  $N$  by

$$\text{FPR}(\tau, N) = 1 - (1 - \text{FPR}(\tau))^N. \quad (6)$$

For further information, we refer to Yang et al. [42, Section 7.1].

## B. Example Images and Image Quality Trade-off

We provide image examples to give more intuition on the attacks and the resulting visual quality. Note that all image examples are of size  $512 \times 512$ , and the attacker’s proxy model is SD2.1. We examine different aspects of the attacks in the following figures:

- Fig. 12 shows the progression of the imprinting forgery attack with respect to the number of optimization steps.
- Fig. 13 shows successful examples of the imprinting forgery attack on different target models and both watermarking approaches (Tree-Ring and Gaussian Shading).
- Fig. 14 depicts successful examples of watermarking removal variant of the imprinting attack.
- Fig. 15 shows successful examples of the reprompting attack.
- Fig. 16 provides a comparison between our removal attack and the AdvEmb attack as baseline.
- Finally, Fig. 17 also presents graphs showing the trade-off between detection rate by the target model and image quality for four combinations of settings: imprinting forgery & removal, and Tree-Ring & Gaussian Shading.

## Imprinting Attack - Progression of Perturbations

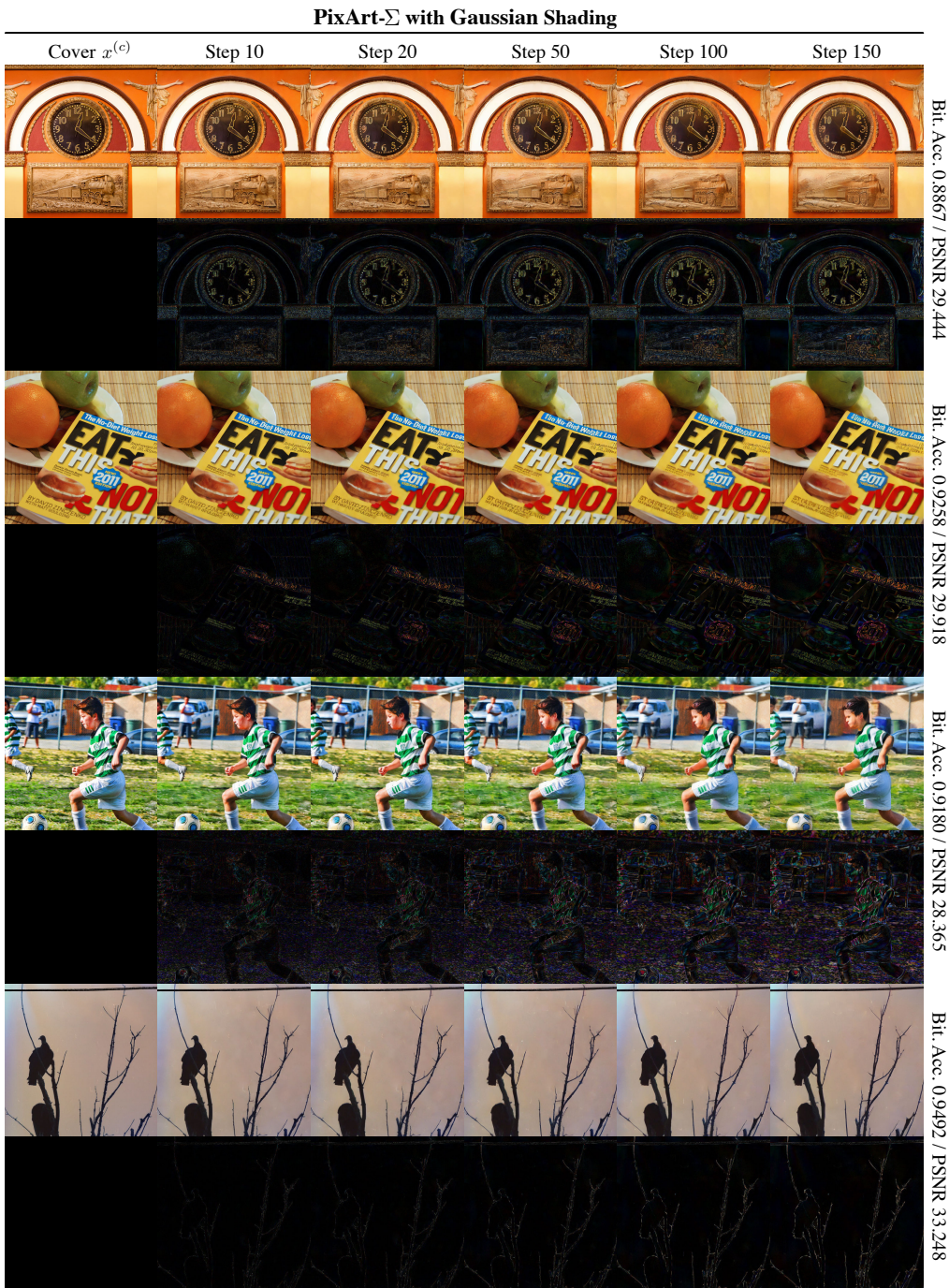


Figure 12. Progression of our imprinting forgery attack with respect to optimization steps. The target model is PixArt- $\Sigma$ , and the forged watermark is Gaussian Shading. Results are presented for four cover images  $x^{(c)}$ . For each cover image, the top row shows the initial cover and then the attack versions after different numbers of optimization steps. The bottom row illustrates the absolute pixel difference between the attack image and its initial cover version. *Observation:* The imprinting attack is targeting edges that carry semantic meaning and reflect unique features in the initial watermarked latent  $z_T^{(w)}$  which we are optimizing towards. Some images with small objects defined by fine characteristics are noticeably changed (small text, small faces), while other features such as the outline of dark objects on bright backgrounds remain almost indistinguishable. The removal attack introduces very similar changes to the images. Note that such critical changes can be avoided simply by using masks during optimization, as described in Sec. 3.

## Imprinting Attack - Successful Examples







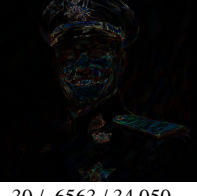
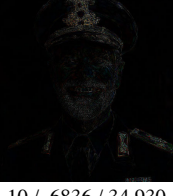
	SD2.1-Anime	SDXL	PixArt- $\Sigma$	FLUX.1	
Step / B. Acc. / PSNR	10 / .8871 / 31.283	10 / .7344 / 31.310	10 / .7265 / 31.313	30 / .7265 / 30.625	
Cover $x^{(c)}$					G. Shading
					Tree-Ring
Step / p-value / PSNR	01 / .0231 / 31.270	30 / .0016 / 30.678	90 / .0146 / 30.456	120 / .0216 / 30.000	
Step / B. Acc. / PSNR	10 / .8906 / 32.544	10 / .7227 / 32.582	10 / .7460 / 32.583	50 / .7500 / 31.207	
Cover $x^{(c)}$					G. Shading
					Tree-Ring
Step / p-value / PSNR	10 / .0012 / 32.576	10 / .0206 / 32.573	30 / .0140 / 31.746	40 / .0160 / 31.353	
Step / B. Acc. / PSNR	10 / .8711 / 32.265	20 / .7851 / 31.6323	20 / .8008 / 31.650	20 / .7344 / 31.610	
Cover $x^{(c)}$					G. Shading
					Tree-Ring
Step / p-value / PSNR	10 / .000 / 32.344	20 / .0148 / 31.568	20 / .0051 / 31.674	60 / .0200 / 30.778	

Figure 13. Examples of our imprinting forgery attack on different target models and both watermark approaches. For each cover image  $x^{(c)}$ , during the different optimization steps, we show the first successful attack image that passes the detection threshold  $\tau$  of Gaussian Shading (FPR  $10^{-6}$ ) or Tree-Ring (FPR 1%). For each image, we report the step, the bit accuracy / p-value, and the PSNR between cover images and attack example. *Observation:* Attacks against PixArt- $\Sigma$  and FLUX.1 usually have stronger visual perturbations, reflecting a higher imprinting difficulty.

## Removal Attack - Successful Examples

SD2.1-Anime	SDXL	PixArt- $\Sigma$	FLUX.1
The image features a young girl with long brown hair, wearing a...	official Portrait of a smiling WWI admiral, male, cheerful, happy, detailed face, 20th century, highly detailed, cinematic lighting, digital art painting by greg rutkowski		

### Gaussian Shading

Watermark				
No Watermark				
Difference				
	20 / .6563 / 31.336	30 / .6328 / 31.895	30 / .6563 / 34.050	10 / .6836 / 34.930

### Tree-Ring

Watermark				
No Watermark				
Difference				
	60 / .0407 / 29.634	40 / .0419 / 31.112	60 / .0348 / 34.111	10 / .3905 / 35.737

Figure 14. Examples of our watermark removal attack on different target models and both watermark approaches. For each target model (column), the 1st row shows the generated, watermarked image  $x^{(w)}$ , the 2nd row the attack example, and the 3rd row the absolute pixel difference between the two. Each attack example is the first one during generation to pass the detection threshold  $\tau$  of Gaussian Shading (FPR  $10^{-6}$ ) or Tree-Ring (FPR 1%). We report the step, the bit accuracy / p-value, and the PSNR between the original and the attack examples. *Observation:* Attacks against FLUX.1 generally display weaker visual perturbations, reflecting a lower removal difficulty.

## Reprompting Attack - Successful Examples


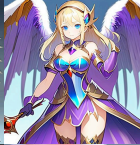




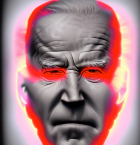












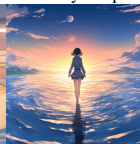





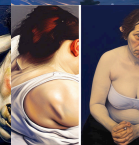

		SD2.1-Anime		SDXL		PixArt- $\Sigma$		FLUX.1	
		G. Shading	Tree-Ring	G. Shading	Tree-Ring	G. Shading	Tree-Ring	G. Shading	Tree-Ring
		The image features a female character with blonde hair, blue eyes...		Pheasant holding a sword, by lily seika jones , rivuletpaper art, very detailed, oil painting, harsh fairy tale, soft style, hyperrealism, beautiful, high resolution, trending on artstation, steps 50					
Original									
Reprompted									
		The image features a young female character with blue eyes, brown hair, and a cat-like headband...		dynamic attack position abstract portrait of a intricate glorious holy mechanical warforged character in yellow armor holding a paladin engraved great longsword drawn and carrying a big paladin shield, glowing!!!! eye!!!!, face in focus, pit droid, epic , trending on ArtStation, masterpiece, cinematic lighting, by Ross Tran and by Greg Rutkowski					
Original									
Reprompted									
		The image features a female character with blonde hair and...		anime girl walking on water, ripples, backdrop of dawn, saturn in the background, illustration, concept art, anime, key visual, trending pixiv fanbox by wlop and greg rutkowski and makoto shinkai and studio ghibli					
Original									
Reprompted									

Figure 15. Examples of the reprompting attack on different target models and both watermarking approaches. In each section, the top row shows benign images which carry a semantic watermark generated with prompts from the **Stable-Diffusion-Prompts** dataset using the respective target model indicated at the top of the figure. The bottom row shows successful attack instances which our reprompting attack generated (using SD2.1 as proxy model) with prompts from the **Inappropriate Image Prompts (I2P)** dataset. Note that we tried to choose less disturbing prompts (without blood, violence, or nudity) for this figure. *Observation:* These results illustrate how an attacker can potentially generate arbitrary harmful images (within the limits of the proxy model) with semantic watermarks spoofed from benign examples to appear as generated by a service or user using the watermarking method.



### FLUX.1 with Tree-Ring

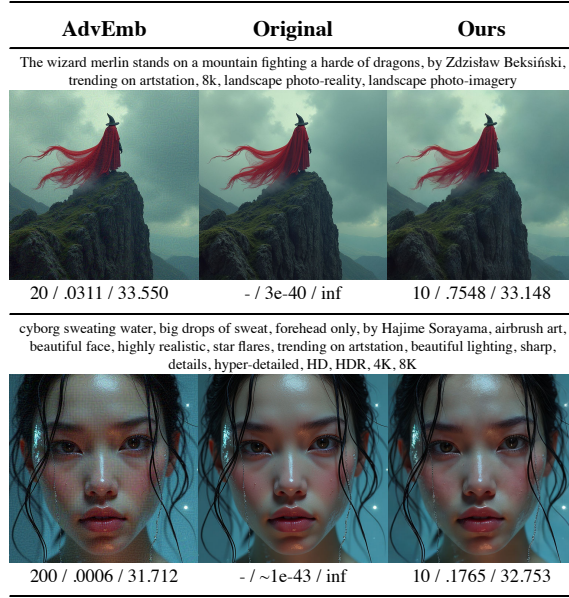


Figure 16. Comparison between our watermark removal attack and the AdvEmb [29] baseline. We focus on removing Tree-Ring watermarks from images generated with FLUX.1, which was the setup where the AdvEmb attack was most effective (see Table 2). For both attacks, we display the first attack instance which passes the detection threshold  $\tau$  @ 1%FPR of 0.02185 (p-value). We report the step at which an attack instance was saved, the p-value, and the PSNR. *Observation:* In the top example, the AdvEmb attack passes the detection threshold early, yet displays a fine-grained but clearly visible adversarial pattern, revealing a possible attack on the watermark. In the bottom example, AdvEmb does not reach the detection threshold even at step 200, while still adding a noticeable pattern. Our attack reaches detection thresholds early and does not introduce any visible patterns.

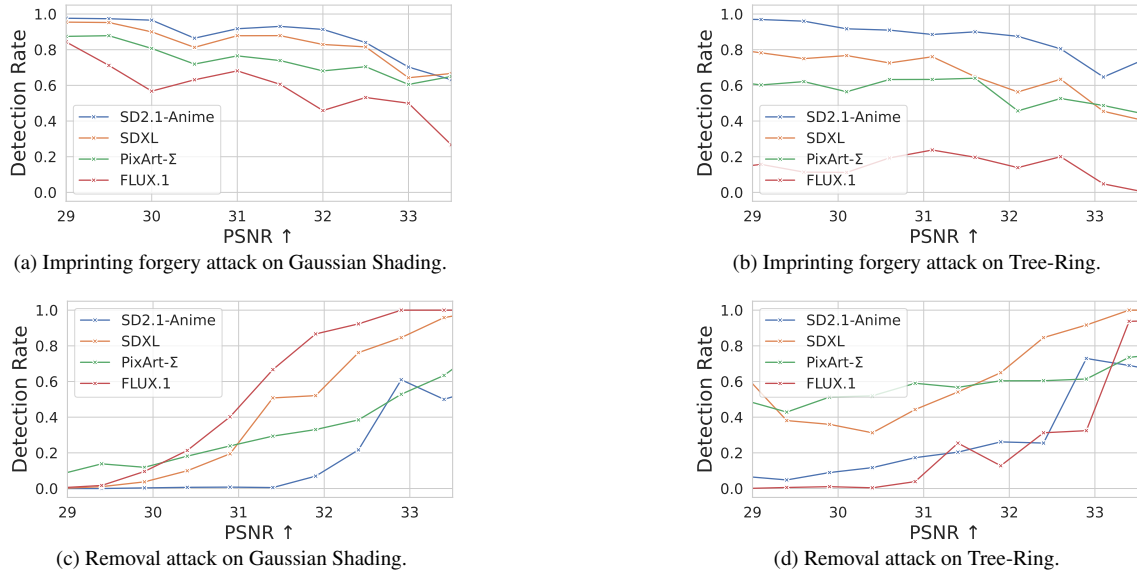


Figure 17. Trade-off between attack success and image quality. To this end, we plot the detection rate vs. PSNR for watermark forgery (top) and removal (bottom) for both watermark approaches (left and right) on different target models. An attacker aims at a higher detection rate in the forgery case, and at a lower detection rate in the removal case. For Gaussian Shading (left), the single-bit detection accuracy is reported with a threshold  $\tau$  corresponding to an FPR of  $10^{-6}$ . For Tree-Ring (right), the detection accuracy is reported with a threshold corresponding to an FPR of 1%. PSNR is computed between the attack image and its initial starting image: the cover image for forgery, and watermarked image for removal. *Observation:* In the case of forgery, we observe a consistent trend where the detection rate increases as image quality decreases. For removal, the detection rate tends to decline rapidly as PSNR decreases.

## C. Experimental Details

Here, we provide more details on our experimental setup, including the datasets used, details on our finetune of Stable Diffusion 2.1 (SD2.1-Anime), the number of samples used in each experiment, the watermark parameters, and the runtime of our attacks.

### C.1. Attacker and Target Models

Our default setup is to use Stable Diffusion 2.1 as the attacker model, and SDXL, PixArt- $\Sigma$ , FLUX.1, and our SD2.1-Anime model as the target models. Our transferability analysis (Sec. 4.5) is the exception where we test multiple combinations of attacker and target models. Tab. 4 provides an overview of all the models used in our experiments, including the scheduler employed and other relevant settings.

Model	Huggingface ID	Type	L. Ch.	Scheduler	I. Steps	G. Scale	G. Shad. Params		
							$\ell$	$\rho$	k
SD1.5	runwayml/stable-diffusion-v1-5	UNet	4	DDIM	50	7.5	1	64	256
SD2.1	stabilityai/stable-diffusion-2-1-base	UNet	4	DDIM	50	7.5	1	64	256
SD2.1-Anime	stabilityai/stable-diffusion-2-1-base	UNet	4	DDIM	50	7.5	1	64	256
SDXL	stabilityai/stable-diffusion-xl-base-1.0	UNet	4	DDIM	50	7.5	1	64	256
PixArt- $\Sigma$	PixArt-alpha/PixArt-Sigma-XL-2-512-MS	DiT	4	DPM	50	7.5	1	64	256
FLUX.1	black-forest-labs/FLUX.1-dev	DiT	16	Euler	20	3.5	1	256	256
Waifu Diffusion	hakurei/waifu-diffusion	UNet	4	DDIM	50	7.5	1	64	256
Mitsua Diffusion One	Mitsua/mitsua-diffusion-one	UNet	4	DDIM	50	7.5	1	64	256
Common Canvas	common-canvas/CommonCanvas-S-C	UNet	4	DDIM	50	7.5	1	64	256

Table 4. Overview of model settings. The settings outlined here are used across all experiments without deviation for both the case that the model at hand is a target model, or the case that it is the proxy model used by the attacker. Image sizes are always set to  $512 \times 512$ . *L. Ch.* refers to the number of latent channels. *Scheduler* refers to the scheduler during image generation and inversion. *I. Steps.* refers to the number of inversion steps during generation and inversion. *G. Scale* refers to the guidance scale during generation. *G. Shad. Params* refers to the Gaussian Shading parameters when the model is deployed as a target model.

### C.2. Prompting and Cover Image Datasets

Except for our SD2.1-Anime model, we use the *Stable-Diffusion-Prompts*<sup>2</sup> dataset to prompt benign watermarked images from the target models for all experiments (Secs. 4.2 to 4.6). For the cover images used in our imprinting forgery attack (Sec. 4.2), we only use the *MS-COCO-2017 Dataset* [20]. In experiments involving our reprompting attack (Secs. 4.4 to 4.6), we use the *Inappropriate Image Prompts (I2P)*<sup>3</sup> dataset (sorting the "inappropriate\_percentage" column in descending order) to generate harmful images with the attacker model.

### C.3. Finetuned Model SD2.1-Anime

Our own finetune of SD2.1 is trained on 10,000 pairs of anime images and captions from the Anime-with-caption-CC0<sup>4</sup> dataset. We use the training scripts for Stable Diffusion models from Huggingface with default parameters for full finetuning of the UNet parameters<sup>5</sup> and for LoRA finetuning<sup>6</sup>. We add a keyword to each caption in the training set and reuse this keyword when generating images during our experiments. For every experiment involving SD2.1-Anime as the target model, we prompt the model with prompts similar to those in the training phase, by taking prompts from a separate split of the same dataset and adding the keywords as prefix. By finetuning our own model, we achieve two goals: First, we obtain a baseline for a target model which is equal to the attacker model (SD2.1) in all aspects except for slight changes in the UNet parameters. This represents a scenario in which a service provider finetunes a publicly available model, and considers the resulting model unique enough to securely deploy semantic watermarks. Second, we are able to quantify the success of forgery attacks at different numbers of training steps for two different finetuning methods (full finetuning and LoRA) (see Sec. F). The model ultimately used in experiments is the fully finetuned variant.

<sup>2</sup>Stable-Diffusion-Prompts

<sup>3</sup>Inappropriate Image Prompts (I2P)

<sup>4</sup>Anime-with-caption-CC0

<sup>5</sup>Huggingface SD training script

<sup>6</sup>Huggingface SD LoRA training script

## C.4. Number of Samples in Experiments

We provide the exact numbers of prompts, generated images, and cover images for all our experiments.

- *Imprinting Attack for Forgery* (Sec. 4.2). We generate 100 images with each target model (using 100 prompts) and apply our imprinting forgery attack on 100 cover images. This adds up to 400 imprinting forgery attacks (100 for 4 target models each) across a fixed set of 100 pairs of prompts and cover images in total. This procedure is performed for both Tree-Ring and Gaussian Shading, doubling the final number of attacks.
- *Imprinting Attack for Removal*, Sec. 4.3. We generate 100 images with each target model (using 100 prompts) and apply our removal attack on each image. This adds up to 400 removal attacks (100 for 4 target models each) across a fixed set of 100 prompts in total. This procedure is done for both Tree-Ring and Gaussian Shading, doubling the final number of attacks.
- *Reprompting Attack*, Sec. 4.4. We evaluate two different variations of our reprompting attack.
  - “Attk”: Here, we generate 1,000 images with each target model using 1,000 benign prompts and reprompt each one with the attacker model using 1,000 harmful prompts. This adds up to 4,000 reprompting attacks (1,000 for 4 target models each) across a fixed set of 1,000 pairs of benign and harmful prompts. This procedure is performed for both Tree-Ring and Gaussian Shading, doubling the final number of attacks.
  - “Attk+ ”: Here, we generate 100 images with each target model using 100 benign prompts. For each image, we reprompt each one 3 times with the attacker model using 300 harmful prompt, for both Tree-Ring and Gaussian Shading. For Gaussian Shading, we further resample the recovered latent  $\hat{z}_T^{(w)}$  for each target image 3 times before reprompting. This adds up to 1,200 reprompting attack for Tree-Ring (300 for each target model, across a fixed set of 100 benign and 300 harmful prompts), and 3,600 reprompting attacks for Gaussian Shading (900 for each target model, across a set of 100 benign and 300 harmful prompts) in total.
- *Transferability Analysis*, Sec. 4.5. For each pair of attacker and target model, we generate 100 images using 100 benign prompts and reprompt each one with the attacker model using a set of 100 harmful prompts. This adds up to 4,900 reprompting attacks (100 for each of the 49 combination of target/attacker model) across a fixed set of 100 pairs of benign and harmful prompts in total. We apply this procedure for Tree-Ring and Gaussian Shading, doubling the number of attacks.
- *No Defense by Adjusting Thresholds*, Sec. 4.6. We reuse the results from Secs. 4.2 and 4.4 as attack instances. Furthermore, we generate 1,000 images with each target model using 1,000 prompts. These are then transformed using common transformations and again verified by the target model. This adds up to an additional 1,000 image generations (1,000 for each of the two target models). We apply this procedure for Tree-Ring and Gaussian Shading, doubling the number.

## C.5. Runtime of Attack Algorithms

All experiments were performed on 8 NVIDIA A40 GPUs. When executed on a single GPU for a single-batch attack example, the approximate runtimes for each attack algorithm are as follows:

- The *imprinting forgery* (Sec. 4.2) and *removal* (Sec. 4.3) attacks require between 25 and 40 minutes to perform 150 steps. The most time-consuming part of these algorithms is the gradient-based optimization done by the attacker model (SD2.1 per default, except for Sec. 4.5). Verification by the target model is set to take place every 10 optimization steps and is comparably fast.
- The *reprompting attack* (Sec. 4.4) requires between 30 seconds (smaller models including SD2.1, Mitsua Diffusion One) and 2 minutes (FLUX.1). This time includes all steps: generating a single image with a semantic watermark on the target model, inverting and regenerating on the attacker model, and verifying the presence of the watermark with the target model.

## C.6. Image Transformations

Fig. 18 shows examples for the standard image transformations that we apply on watermarked images to examine the achievable thresholds of Tree-Ring and Gaussian Shading under these transformations (cf. Sec. 4.6 and Sec. E).

## C.7. Parameters for Tree-Ring and Gaussian Shading

In order to run Gaussian Shading and Tree-Ring, several parameters need to be selected.

**Tree-Ring.** In the original work of Wen et al. [38], the threshold for the p-value to assume the watermark’s presence is computed by calculating receiver operating characteristics (ROC) curves. For their main results, they report AUROC and TPR@FPR=1%. As precise p-values are not reported, we conduct our own experiment similar to the original work. For each model evaluated, we generate 5,000 watermarked images as well as 5,000 clean images to determine the thresholds for desired



Figure 18. Examples of common image transformations

FPRs. The thresholds for 10%, 1%, and 0.1% FPR are reported in Tab. 5. We kept all other parameters of the scheme as provided in the implementation of the authors<sup>7</sup>.

**Gaussian Shading** [42] requires the user to set the message length  $k$ , the repetition factor  $\rho$ , and the number of bins  $2^\ell$  to sample from a Gaussian distribution. The system was originally evaluated for SD2.1-like 4-channel latents with a scaling factor of 8 (i.e.  $4 \times 64 \times 64$  for images of size  $512 \times 512$ ). Ideal parameters for this size were experimentally determined by Yang et al. [42] as  $k = 256$ ,  $\rho = 64$ , and  $\ell = 1$ . In Tab. 6, we provide detection thresholds  $\tau$  for both zero-bit and multi-bit scenario for a desired FPR according to Eq. (6) (with  $N = 1$  in case of zero-bit). Given  $k = 256$ , the detection threshold for a FPR of  $10^{-6}$  is 0.64844 for a zero-bit scenario. Assuming  $k = 256$  and  $N = 100,000$  in line with Yang et al. [42], the detection threshold  $\tau$  is set at 0.70703 for a multi-bit scenario. Throughout our work, we always assume this multi-bit scenario, meaning we use a definitive Gaussian Shading detection threshold of  $\tau = 0.70703$  above which an image is recognized as watermarked. User attribution was done as described in Sec. 4: For each image to be attributed, first, the user id with the highest number of matching bits from a pool of  $N = 100,000$  randomly generated users is retrieved. Then, if the number of matching bits exceeds  $\tau$ , the sample is counted as attributed to this user. Our results regarding successful user attribution in Tabs. 1 to 3 always match the detection success because of small sample sizes, making it improbable for another user to match the bit string at hand and also pass the detection threshold.

In order to adapt the scheme to models like FLUX.1 with 16-channel latents (and the same scaling factor of 8), we have to adjust the parameters. We choose to use the same message length with a higher repetition factor  $\rho$ . A higher repetition factor makes the scheme more robust to bit-errors and therefore to perturbations. Using the same message length lets us keep thresholds  $\tau$  unchanged regardless of the dimensions of the latent. We consider this to be at least as hard to attack as alternative adjustments, as increasing the message length will also yield lower detection thresholds in return as the probability of randomly drawing correct bit-strings of larger size decreases significantly. For example, using  $k = 512$  would lower the thresholds for an FPR of  $10^{-6}$  to 0.60547 (zero-bit) and 0.64648 (multi-bit), which would make watermark removal slightly harder but imprinting and reprompting slightly easier.

In Tab. 4, we report our parameters for Gaussian Shading for multiple models with different latent sizes.

FPR	SD2.1-Anime	SDXL	PixArt- $\Sigma$	FLUX.1
10%	0.14275	0.13493	0.15809	0.14287
1%	<b>0.02466</b>	<b>0.02610</b>	<b>0.01591</b>	<b>0.02185</b>
0.1%	0.00555	0.00553	0.00048	0.00074

Table 5. Thresholds  $\tau$  in terms of p-value for Tree-Ring for multiple FPRs and models. The thresholds used in our work are marked in bold.

FPR	Zero-bit Threshold	Multi-bit Threshold
$10^{-6}$	0.64844	<b>0.70703</b>
$10^{-16}$	0.75000	0.78906
$10^{-32}$	0.85156	0.87500
$10^{-64}$	0.97266	0.98438

Table 6. Thresholds  $\tau$  in terms of bit accuracy for Gaussian Shading, zero-bit and multi-bit configurations ( $N = 100,000$  users) with a watermark capacity  $k = 256$  at various FPR levels for all models. The threshold used in our work is marked in bold.

<sup>7</sup>Github Repository of Tree-Ring

## D. Transferability Analysis

In this section, we present additional data for our transferability analysis from Sec. 4.5 by looking at the similarity of auto-encoders.

We evaluate the similarities of different VAEs, since all our models tested in Sec. 4.5 deploy VAEs with 4 latent channels and the same order of layers. We first examine the weights of the different autoencoders across the different models. SD2.1 and Common Canvas appear to share the exact same VAE, as all weights of all layers match with a precision of  $10^{-3}$ . Next, we examine if some of the VAEs are functionally similar by comparing their latents for a set of images. We use a random sample of 100 images from the MS-COCO-2017 dataset [20], for which we compute latent embeddings using a VAE’s encoder, and compare the representations obtained by different autoencoders using cosine similarity.

The functional similarities are reported in Fig. 19. We observe that SD2.1, SD1.5, Waifu Diffusion, and Common Canvas have very similar latents accross all test images. In addition, we observe that SDXL and PixArt- $\Sigma$  share a similar VAE as well. Mitsua’s autoencoder appears to behave differently from the other VAEs, which supports the claim that Mitsua’s VAE was trained from scratch stated on the corresponding Huggingface model card<sup>8</sup>. Comparing these results to Fig. 10 (which are also displayed in the figure below for convenience) reveals that latent encoder similarity correlates with high transferability, but does not explain it entirely. For example, Mitsua and Common Canvas have quite dissimilar autoencoders but still transfer easily in our reprompting experiments. Also note that the heatmaps are almost symmetrical.

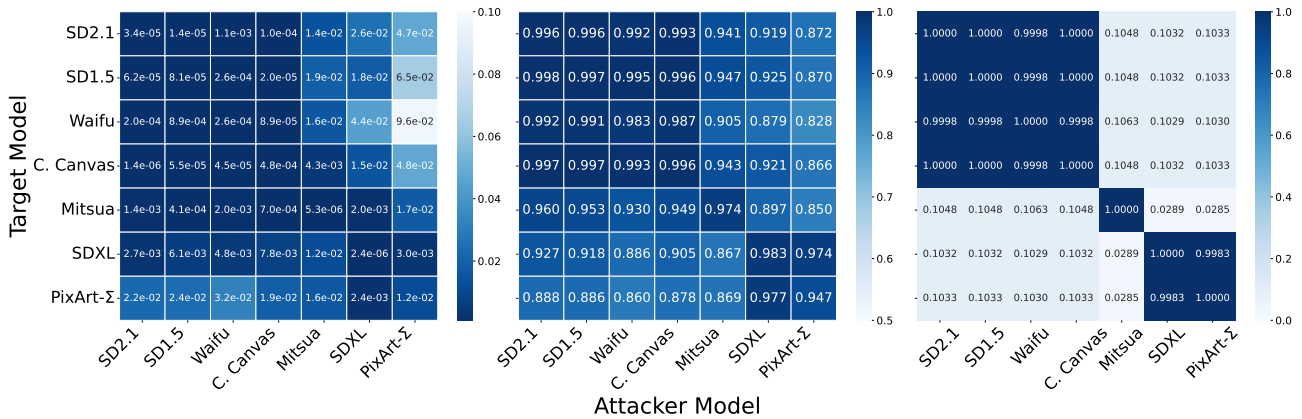


Figure 19. Transferability across different pairs of target and attacker model. For convenience, the left plot shows the reprompting transferability for Tree-Ring in terms of p-value ( $\downarrow$ ), and the middle plot for Gaussian Shading in terms of bit accuracy ( $\uparrow$ ). The right plot shows the functional analysis of autoencoders. Function similarity is measured as averaged cosine similarity between latents of different autoencoders for 100 different images.

<sup>8</sup>Mistua Diffusion One Huggingface model card

## E. A Side-note on Robustness

Fig. 20 provides further intuition on possible thresholds (Fig. 9) by showing additional transformations and settings. We can identify a notable vulnerability of the watermarking methods to some common perturbations. Gaussian Shading is especially vulnerable to cropping, scaling, and rotation. The p-values in Tree-Ring are significantly affected by crop-and-scale operations. Any transformation that changes the location of pixels destroys the watermark. In contrast, deleting parts of the image preserves the watermark, as enough pixels are still in the correct position. It appears that Gaussian Shading requires the image to be in the same position with which it was generated, which might not be a viable assumption in practical deployment. This illustrates that these watermarks can be easily removed and that further research into more robust semantic watermarking methods is necessary.

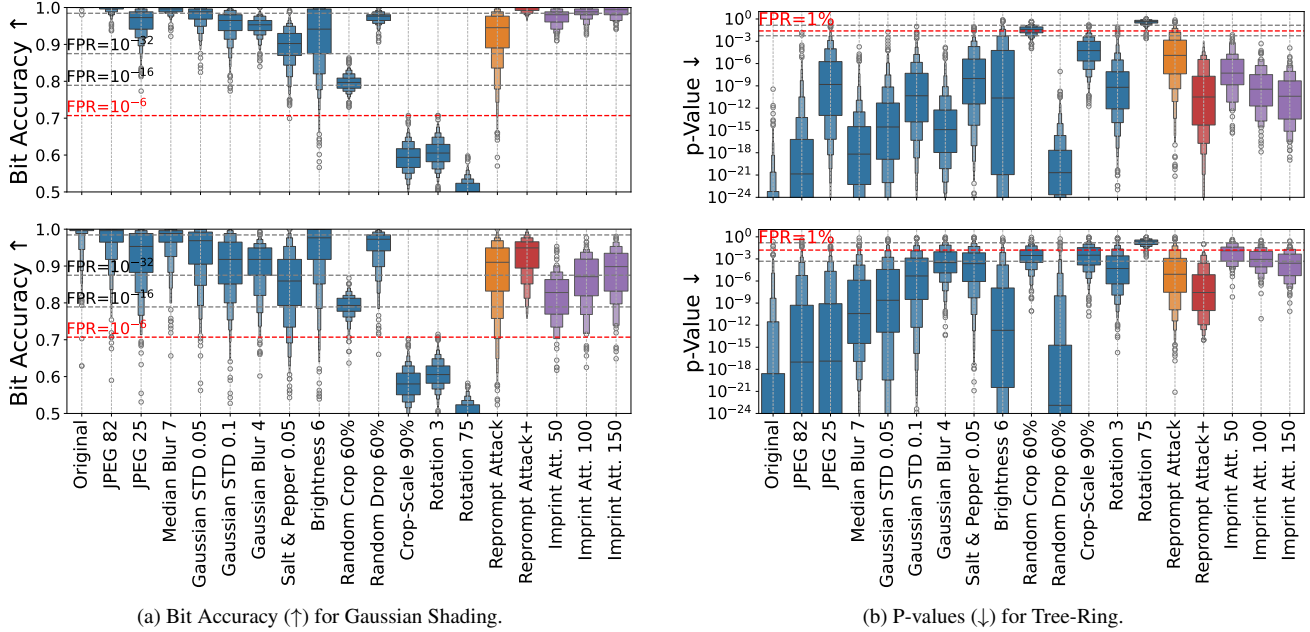


Figure 20. Comparison between image perturbations (blue bars) and our attacks (orange, red and purple bars), for Gaussian Shading (left) and Tree-Ring (right). Orange bars are the reprompting attack, red bars are enhanced reprompting attack, purple bars are imprinting attack for different numbers of optimization steps. Results are shown for two target models: SD2.1-Anime (top) and PixArt- $\Sigma$  (bottom). We can observe that no threshold can effectively separate images from common transformations and attacks.

## F. Attack Success vs Training Steps

For different amounts of finetuning steps of our SD2.1-Anime finetune, Fig. 21 shows bit accuracies and p-values achieved with our reprompting attack on Gaussian Shading and Tree-Ring, respectively. The attacker model is SD2.1.

The attack effectiveness decreases with longer finetuning, as expected. However, the longer the target model is trained, the slower the rate of decrease. In our experiment, the attack metrics seems to stabilize after around 4k training steps, still crossing most detection thresholds. Importantly, the bit accuracy for the attack images exceeds the detection threshold set at  $FPR=10^{-6}$  (the threshold from the original paper, marked in red in Fig. 21). Similarly, for Tree-Ring, the p-values fall below the detection threshold for the  $FPR=1\%$  setting from the original paper (marked in red).

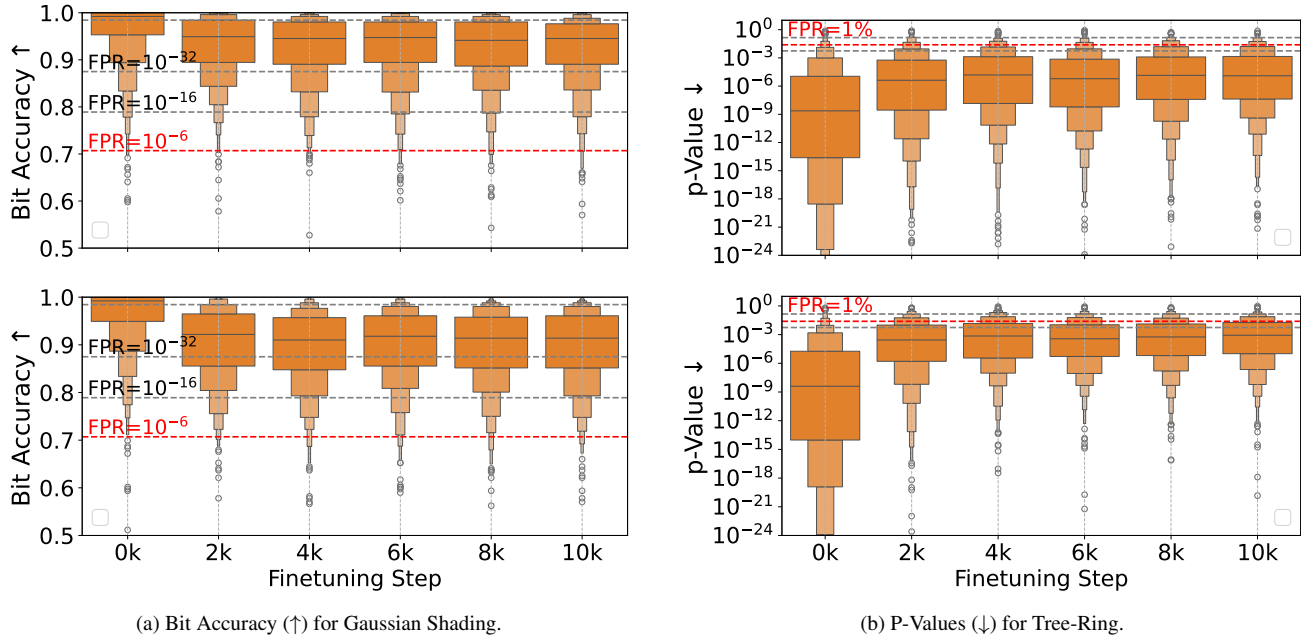


Figure 21. Performance of the reprompting attack for Gaussian Shading (left, measured using bit accuracy) and Tree-Ring (right, measured using p-value), after different numbers of finetuning of our SD2.1-Anime model. Numbers are reported both for regular full finetuning (top), as well as finetuning using LoRA (bottom). We can observe from the results that no threshold can effectively separate images from common transformations and attacks. Marked dashed red lines are the thresholds used in the original papers, corresponding to an FPR of  $10^{-6}$  for Gaussian Shading and FPR of 1% for Tree-Ring watermarks.